MODELING CONVECTIVE COOLING APPLIED TO PERFUSED AND NON-PERFUSED LAYERS USING THERMAL MEASUREMENTS (WITH AND WITHOUT THERMAL CAPACITANCE EFFECTS)

Abdusalam Alkhwaji

AL Asmarya Islamic University, College of Engineering, Zliten, Libya
a.alkhwaji@asmarya.edu.ly

ABSTRACT

Thermal measurements are collection of data which are either heat flux or temperature data. Thermal measurements have been used in detecting distribution of heat transfer through the boundary of a thermal system; as an example, the case of modeling burn depth, or skin cancer, etc., where damaged tissue suffers dysfunction perfusion process. Damaged tissue causes blood perfusion either to increase (inflammation process) or decease (burns). In this study, an investigation was carried out to develop an optimal modeling method to simulate heat transfer through a compartment of non-perfused and perfused layers. The first model was one-Layer compartment (thermal resistance model), in which the effect of thermal capacitance of the non-perfused layer was not counted for. The second model was two-layer compartment (perfused and non-perfused layers), in which the effect of thermal capacitance of non-perfused layer was included.

For the one-layer compartment model, a numerical solution was developed based on finite difference method to describe heat transfer through a perfused layer. This one-layer compartment finite difference solution has perfusion effect and without thermal capacitance effect. The non-perfused layer was represented in the one-layer FD-solution explicitly as thermal resistance. For the two-layer compartment model, another finite difference solution was used to describe the two layers along with the thermal capacitance effect. The results of this investigation demonstrate that by modeling with thermal resistance of a non-perfused layer, the complexity in handling two-layers is going to be reduced, and the estimated parameters of both models was close.

Keywords: thermal measurements; modeling thermal system; thermal capacitance effect

1. INTRODUCTION

An optimal model minimizes complexity and speeds the search for unknown thermal system parameters. Representing a non-perfused layer as a thermal resistance eliminates the need to discretize the non-perfused layer (Numerical approaches). The thermal resistance model smooths the thermal system boundaries and that makes it easier to derive an analytical solution for two inhomogeneous layers (perfused and non-perfused layers).

These methods have significant usage in thermal research; such as for counting for thermal insulation of a soil-layer flowing above a river. Another application of this research is in building a medical diagnostic device; where the heat transfer through a tissue can be used to monitor and detect any abnormality in perfused flow (Blood perfusion). The perfused flow in most thermal system is a heat carrier; as an example, the amount of thermal energy transported by blood indicates the status of the tissue. In living tissue (Perfused layer), blood perfusion delivers oxygen and nutrients to the cells while rejecting wastes and heat.

The goal of the present research is to evaluate two thermal models of a non-perfused layer. The one-Layer compartment finite difference model which has no thermal capacitance effect is tested versus the two-Layer compartment finite difference model which includes thermal capacitance effects.

2 .EXPERIMENTAL THERMAL MEASUREMENT METHODS

2.1 TISSUE SIMULATOR (PHANTOM TISSUE)

Experimental measurements were obtained with the temperature-heat flux sensor using the Phantom Tissue System of Mudalier et al. [14]. This test stand is designed to supply perfusate into the tissue simulator at a controlled temperature and flow rate. The bottom area of the tank stores water maintained at a constant 37 ℃ temperature (core body temperature) by a temperature controller in conjunction with a cartridge heater. The perfusate flow is provided by a small centrifugal pump from the water bath directly through a flowmeter into the porous matrix which acts as the tissue simulator.

2.2 TEMPERATURE-HEAT FLUX SENSOR

Thermal measurements are collected using temperature-heat flux sensor, where the heat flux sensor is a BF-02 heat flux gage (from Vatell company), which has sensitivity of 2.1 mV/ (W/cm^2). This is a 0.25-mm thick thermopile-based heat flux sensor. The coupled temperature-heat flux sensor is a completely sealed sensor (0.28-mm thick) with a thin-film thermocouple next to the test material, as illustrated in Fig. 1. This coupled temperature and heat flux sensor provides direct measurement of heat flux and temperature between the non-perfused layer and sensor, as well as a water tight seal to protect the sensor from moisture present in tissue.

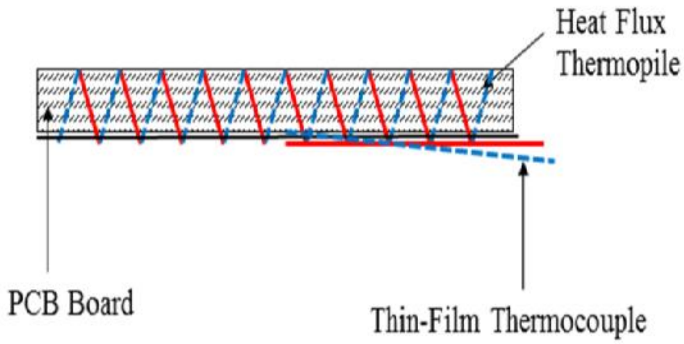

Figure 1 Combination Heat Flux/Temperature Sensor

2.3COOLING SURFACE OF NON-PERFUSED LAYER

Initially the thermal system (perfused and non-perfused layers) is thermally in equilibrium with the tissue simulator (Phantom Tissue), which provides continually the perfused layer with an internal heating source (perfusion carrying heat with a constant core temperature).

As forced convective cooling (advection) is applied at non-perfused surface (Boundary of the thermal system), the surface of non-perfused layer starts to excide the steady state behavior. The non-perfused disturbed layer will try to replace the rejected energy during convective cooling process. Heat transfer rate through perfused layer is faster than that through a non-perfused layer; therefore, it is possible to detect thickness of non-perfused layer. Thickness of non-perfused layer can be detected by measuring heat rate rejected through surface. That is exactly what happens when burn is initiated, the thickness of non-perfused layer (dead tissue) increase, and heat transfer rate is going to be diminished.

The amount of heat flux and the time required to return the thermal system (tissue) to its original equilibrium (steady state), are an indication of any additional non-perfused layer (tissue abnormality). These results can be used as a diagnostic tool to detect thickness of an abnormal tissue, where the amount of blood perfusion controls the time required to reach back the equilibrium condition.

In the designed forced convective cooling (thermal event), cold air is provided by nine jets of room temperature onto the top side of the temperature-heat flux sensor. The jets are created with a compressed air supply through 0.37 mm holes. When the jets are turned on, the sudden increase in convection gives a corresponding increase in rejected heat transfer from the non-perfused surface through the temperature-heat flux sensor and the thermal contact resistance, as illustrated physically in Fig. 2. The experimental temperature and heat flux measurements are recorded with a 24-bit DAQ at sampling rate of sample per second.

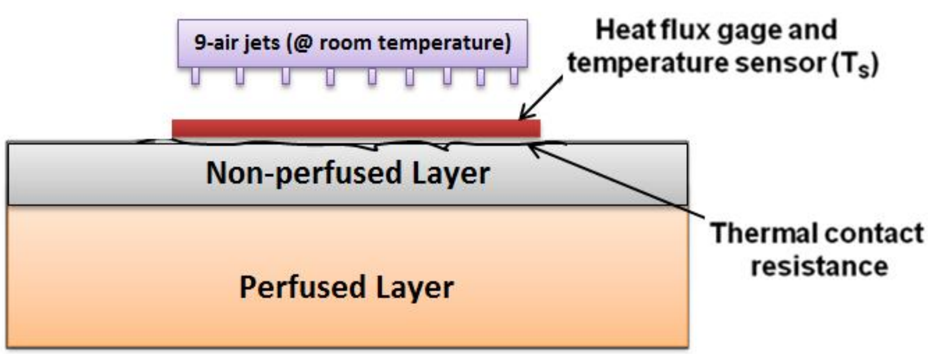

Figure 2 System model

2.4 MODELING COOLING OF SURFACE OF NON-PERFUSED LAYER

Modeling cooling of perfused and non-perfused layers is done by applying energy conservation theorem around the two layers. Where for a biological thermal system, the top layer simulates a damaged tissue (burn,skin cancer, etc.); while the bottom layer represents a healthy tissue (perfused tissue).The dynamical cooling is expressed at the surface boundary as;

$$-\boldsymbol{k}\frac{\boldsymbol{\partial}}{\boldsymbol{\partial}}|_{x=0} = \frac{\mathbf{1}}{\boldsymbol{R'}}\left(\boldsymbol{T_S}(\boldsymbol{t}) - \boldsymbol{T}(\mathbf{0},\boldsymbol{t})\right) \qquad \textbf{(1)}$$

While the continued internal perfusion heat source provides the far boundary condition as;

$$\frac{\boldsymbol{\partial}}{\boldsymbol{\partial}}|_{x\to\infty} = \mathbf{0} \qquad \textbf{(2)}$$

For this study the Pennes equation (3) is considered in one dimension and simplified by the assumption of the equality of perfused layer (tissue) and blood (perfused flow). Also all properties are taken with average values [20, 21] where k_t = 0.5 W/m-K, ρ_t = 1050 kg/m^3, and $c_{p,t}$ = 3800 J/kg-K. The thermal diffusivity is defined as $\alpha = (k/\rho\ \ )_t = (k/\rho\ \ )_b$

The one-dimensional transient bioheat equation in the x-direction:

$$\frac{\partial}{\partial} = \alpha\frac{\partial^2 T}{\partial x^2} - w_b(T - T_c\ \ \ ) \qquad \textbf{(3)}$$

where the terms; w_b is perfusion, and $w_b(T\text{-}T_{core})$ represents the continued internal perfusion heat source. Figure 3 illustrates tissue simulator (compartment of two-layers perfused & non-perfused), and the corresponding boundary conditions. The non-perfused layer is a sheet of plastic, while the perfused layer is a sponge (water perfused through it with a controlled amount). The thermal contact resistance between the sensor and plastic layer is represented by R''_0, while the thermal resistance of the plastic layer is $R''_p = L/k_p$. L and k_p are thickness and thermal conductivity of the plastic layer, respectively.

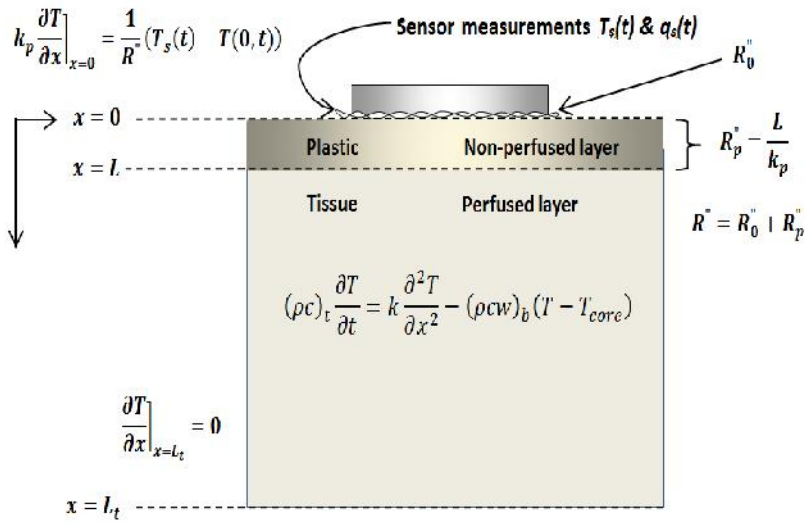

Figure 3 modeling a simulated two-layer compartment.

The non-perfused layer is either expressed as an additional thermal resistance neglecting its thermal capacitance or as an additional layer with all of the plastic properties. The one-compartment finite difference solution treats the problem as one layer with an added thermal resistance. The one-compartment model lumps two thermal resistances R''_0 and R''_p together and only solves the full transport equation in the tissue compartment. The two compartments model solves equation 3 in both layers, using zero perfusion and appropriate thermal properties in the plastic layer. The details of the solution techniques and results are given in the following sub-sections. The shifting variable $\theta = T - T_{core}$ is going to be used in equation 1, 2, and 3 instead of T. Where θ_i means $T_i - T_{core}$.

3. ONE-LAYER COMPARTMENT FINITE DIFFERENCE MODEL

Before the convective forced cooling is initiated by turning on the air jets, the heat flux at the surface is balanced by the warmed perfused flow in the simulated tissue. The initial steady-state temperature distribution in the perfused layer (tissue) $\boldsymbol{\theta_i}$(x) is obtained by solving analytically the steady-state version of equation 3 along with the boundary conditions from equation 1 and 2 [6]

$$\boldsymbol{\theta_i(x) = \theta(x,0) = \frac{\theta_S(t_0)}{\left[k\,R''\sqrt{\frac{w_b}{\alpha}}+1\right]} e^{-\sqrt{\frac{w_b}{\alpha}}\,x}} \quad \textbf{(4)}$$

Where the initial sensor temperature is $\boldsymbol{\theta_S(t_0)}$.

The one compartment model makes use of two solutions, which are the transient and steady-state solutions of equation (3). The initial heat flux is calculated from the first derivative of equation (4).

$$\boldsymbol{q_i(x=0) = -k\theta_S(t_0)\left[\frac{\sqrt{w_b/\alpha}}{1+R''k\sqrt{w_b/\alpha}}\right]} \tag{5}$$

where the initial sensor temperature minus the core temperature is$\boldsymbol{\theta_S}$**(t$_0$).** The transient heat flux describes the response to the forced convective cooling event.

The numerical solution to the 1D bioheat equation using Crank Nicolson approach (n, i) - indicates respectively the indexes of time and space). Figure 4 illustrates the finite difference discretization of the thermal system.

Discretizing the Contact Resistance layer;

$$\frac{k_t}{\Delta x}\left[\theta_{t,1}^{n} - \theta_{t,2}^{n}\right] = \frac{\left(\theta_m^n - \theta_{t,0}^n\right)}{R''} \tag{6}$$

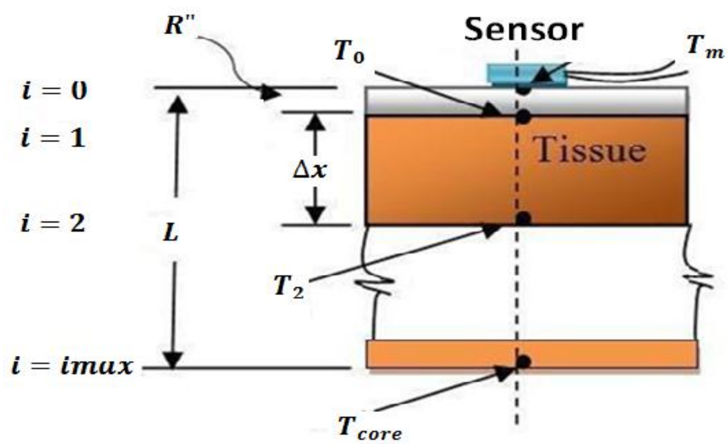

Figure 4 discretizing the finite difference model

Discretizing the region between the core body temperature and the Contact Resistance layer

$$\frac{\theta_{t,i}^{n+1}-\theta_{t,i}^{n}}{\Delta t}=\alpha_t\frac{\theta_{t,i+1}^{n+1}-2\theta_{t,i}^{n+1}+\theta_{t,i-1}^{n+1}+\theta_{t,i+1}^{n}-2\theta_{t,i}^{n}+\theta_{t,i-1}^{n}}{2\Delta x^2} - \beta\left(\frac{\theta_{t,i}^{n+1}+\theta_{t,i}^{n}}{2}\right) \quad \textbf{(7)}$$

Taking $\vartheta_t = 2\Delta x^2$ & $\alpha_t = \frac{k_t}{\rho c_{p,t}}$, $\beta = \frac{\rho c_b}{\rho c_{p,t}} w_b = w_b$, where subscript "t" indicates tissue (perfused layer). The region between the two boundary conditions; $2 \le i \le tmax - 2$, the equation is

$$(2\alpha_t\Delta t-\vartheta_t+\beta\Delta t\Delta x^2)\theta_{t,i}^{n}-\alpha_t\Delta t\theta_{t,i+1}^{n}-\alpha_t\Delta t\theta_{t,i-1}^{n} = \alpha_t\Delta t\theta_{t,i+1}^{n+1}-(2\alpha_t\Delta t+\vartheta_t+\beta\Delta t\Delta x^2)\theta_{t,i}^{n+1} + \alpha_t\Delta t\theta_{t,i-1}^{n+1} \quad \textbf{(8)}$$

At the surface of the non-perfused layer at (i = 1)

$$(2\alpha_t\Delta t-\vartheta_t+\beta\Delta t\Delta x^2)\theta_{t,1}^{n}-\alpha_t\Delta t\theta_{t,2}^{n}-\alpha_t\Delta t\theta_{t,0}^{n} = \alpha_t\Delta t\theta_{t,2}^{n+1}-(2\alpha_t\Delta t+\vartheta_t+\beta\Delta t\Delta x^2)\theta_{t,1}^{n+1} + \alpha_t\Delta t\theta_{t,0}^{n+1} \quad \textbf{(9)}$$

The faraway boundary condition at $i = tm \quad - 1$

$$(2\alpha_t\Delta t-\vartheta_t+\beta\Delta t\Delta x^2)\theta_{t,t\quad -1}^{n}-\alpha_t\Delta t\theta_{t,t\quad}^{n}-\alpha_t\Delta t\theta_{t,t\quad -2}^{n} = \alpha_t\Delta t\theta_{t,t\quad}^{p+1}-(2\alpha_t\Delta t+\vartheta_t+\beta\Delta t\Delta x^2)\theta_{t,t\quad -1}^{n+1} + \alpha_t\Delta t\theta_{t,t\quad -2}^{n+1} \quad \textbf{(10)}$$

Where: $\theta^{n}_{t,t} = \theta^{n+1}_{t,t} \quad x = 0$

Finite difference heat flux for the one-Layer compartment:

$$q_s^{n+1} = \frac{(\theta_{0,t}^{n+1} - \theta_s^{n+1})}{R_0'} \tag{11}$$

$\theta_m^p = f(t)$, is the measured temperature above the contact resistance layer. These equations are coded in Matlab and solved simultaneously using Tomas algorithm.

1. TWO-LAYER COMPARTMENT FINITE DIFFERENCE MODEL

The two-compartment model includes the thermal contact resistance with capacitance in the plastic layer. Consequently, the first two boundary conditions for the two-compartment model are the same as for the one-compartment model. The last two are specific to the added plastic layer. Figure 5 illustrates the two-layer compartment model.

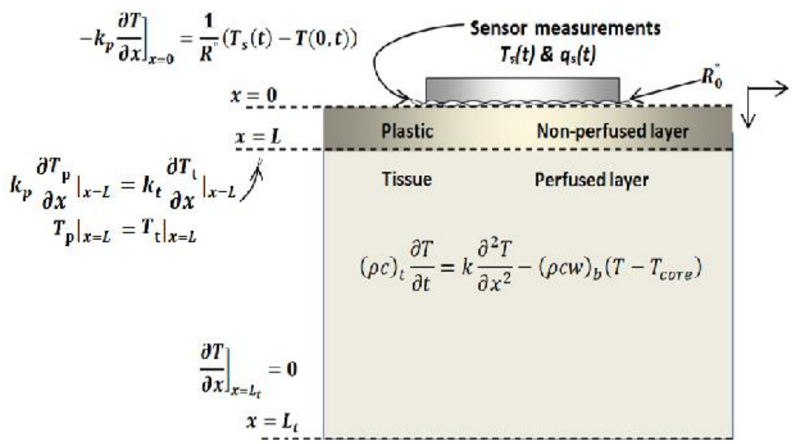

Figure 5 modeling a simulated two-Layer compartment

$$\frac{\partial \theta_t}{\partial}|_{x \to L_t} = 0 \qquad \textbf{(12)}$$

$$-k_p \frac{\partial \theta_p}{\partial}|_{x=0} = \frac{1}{R''}\left(\theta_S(0) - \theta_p(0,0)\right) \qquad (13)$$

$$k_p \frac{\partial \theta_p}{\partial}|_{x=L} = k_t \frac{\partial \theta_t}{\partial}|_{x=L} \qquad (14)$$

$$\theta_p|_{x=L} = \theta_t|_{x=L} \qquad (15)$$

Where subscript *t* is for sponge (perfused layer) and subscript *p* is for plastic (non-perfused layer) ($wb = 0$). Because the sponge has perfused flow, there is a non-linear temperature gradient in the sponge at steady-state conditions. Therefore, the proper steady-state solution of equation (3) is required to initiate the finite-difference solutions for the two models. For the one-layer compartment the initial temperature distribution is given by equation (4). For the two-layer compartment the initial temperature distribution is derived by solving the steady-state version of equation (3) with the boundary conditions in equations (12-15). The steady-state form of equation (3) is

$$\frac{\partial^2 \theta}{\partial x^2} - m \quad = 0 \qquad (16)$$

where $m = \sqrt{\rho \ w_b / k_t}$. The corresponding solution for the perfused compartment (simulated tissue) is

$$\boldsymbol{\theta_t(x) = A\,s\quad (m\quad) + B\,c\quad (m\quad)} \tag{17}$$

$$\boldsymbol{A = -\frac{\left[1 + \frac{L}{k_p R''}\right] C_2 - \frac{L}{k_p R''}\theta_s(0)}{c\quad (m\quad) - t\quad \big(m(L + L_t)\big)\, s\quad (m\quad)}\, t\quad \big(m(L + L_t)\big)} \tag{18}$$

$$\boldsymbol{B = \frac{\left[1 + \frac{L}{k_p R''}\right] C_2 - \frac{L}{k_p R''}\theta_s(0)}{c\quad (m\quad) - t\quad \big(m(L + L_t)\big)\, s\quad (m\quad)}} \tag{19}$$

For the plastic compartment (non-perfused layer) the solution is linear and matched with the heat flux and temperature at the interface between the two compartments.

$$\boldsymbol{\theta_p(x) = C_1 x + C_2} \tag{20}$$

$$\boldsymbol{C_1 = -\frac{1}{k_p R''}\left(\theta_s(0) - C_2\right)} \tag{21}$$

$$\boldsymbol{C_2 = \frac{\theta_s(0)D - \frac{L}{k_p R''}\theta_s(0)F}{D - \left[1 + \frac{L}{k_p R''}\right]F}} \tag{22}$$

$$\boldsymbol{D = \frac{\frac{1}{R'' m k_t}}{\left[s\quad (m\quad) - t\quad \big(m(L + L_t)\big)\, c\quad (m\quad)\right]}} \tag{23}$$

$$F = \frac{1}{c\quad(m\ ) - t\quad\big(m(L + L_t)\big)\, s\quad(m\ )} \tag{24}$$

The initial solution is built from two solutions for the two-compartments.

$$\theta_i(x) = \begin{Bmatrix} \theta_p(x) & x \le L \\ \theta_t(x) & L < x \le L_t \end{Bmatrix} \tag{25}$$

Figure 6 illustrates the initial temperature distribution of the two finite-difference models for an example of plastic layer of Lexan with a 0.381 mm thickness. The initial temperature distribution in the plastic is linear since the perfused flow term is zero, while the (perfused) sponge region has perfused flow. The coordinate x is from the surface of the model. The added thermal resistance of the plastic layer lowers the surface temperature.

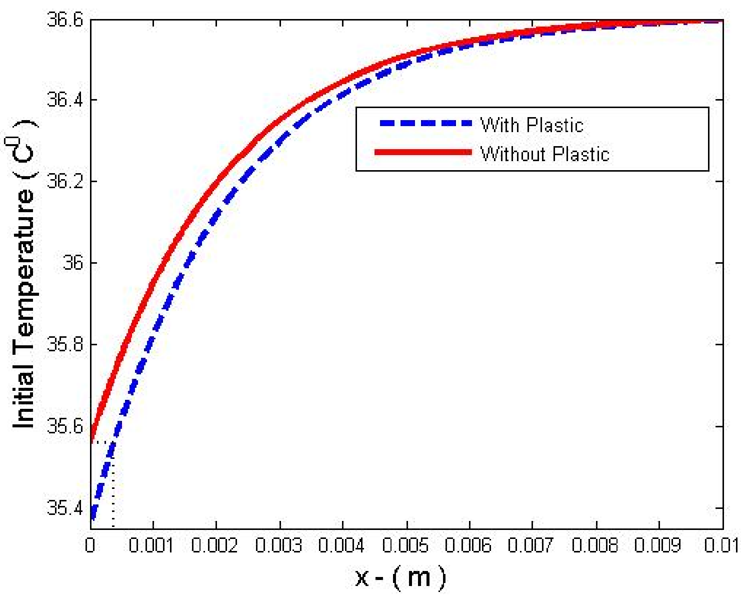

Figure 6 Initial temperatures for one-compartment and two-compartment models of 0.381 mm-plastic

The transient finite-difference scheme uses the Crank Nicolson method [17]. The stability of space and time meshing was tested for the 0.381 mm Lexan example, where total of 20,000 nodes were used in the x-direction with a uniform spacing for both plastic and sponge. The sponge thickness was set at $L_t = 2\,c$. The time step was Δt =1 s. The results were unaffected when the size of Δt and Δx were varied by a factor of ten.

Discretizing the two compartment models

For non-perfused layer

$$\frac{\theta_{p,i}^{n+1}-\theta_{p,i}^{n}}{\Delta t} = \alpha_p \frac{\theta_{p,i+1}^{n+1}-2\theta_{p,i}^{n+1}+\theta_{p,i-1}^{n+1}+\theta_{p,i+1}^{n}-2\theta_{p,i}^{n}+\theta_{p,i-1}^{n}}{2\Delta x^2} - \beta\left(\frac{\theta_{p,i}^{n+1}+\theta_{p,i}^{n}}{2}\right) \tag{26}$$

Taking $\vartheta_p = 2\Delta x^2 \& \alpha_p = \frac{k_p}{\rho c_{p,p}}$, $\beta = \frac{\rho c_b}{\rho c_{p,p}} w_b = w_b$, where subscript "p" indicates plastic (non-perfused layer) . For the region between the two boundary conditions; $2 \le i \le pmax - 2$, the equation is

$$(2\alpha_t\Delta t - \vartheta_t + \beta\Delta t\Delta x^2)\theta_{t,i}^{n} - \alpha_t\Delta t\theta_{t,i+1}^{n} - \alpha_t\Delta t\theta_{t,i-1}^{n} = \alpha_t\Delta t\theta_{t,i+1}^{n+1} - (2\alpha_t\Delta t + \vartheta_t + \beta\Delta t\Delta x^2)\theta_{t,i}^{n+1} + \alpha_t\Delta t\theta_{t,i-1}^{n+1}$$

$$\left(2\alpha_p\Delta t - \vartheta_p + \overbrace{\beta}^{0}\Delta t\Delta x^2\right)\theta_{p,i}^{n} - \alpha_p\Delta t\theta_{p,i+1}^{n} - \alpha_p\Delta t\theta_{p,i-1}^{n} = \alpha_p\Delta t\theta_{p,i+1}^{n+1} - \left(2\alpha_p\Delta t + \vartheta_p + \overbrace{\beta}^{0}\Delta t\Delta x^2\right)\theta_{p,i}^{n+1} + \alpha_p\Delta t\theta_{p,i-1}^{n+1} \tag{27}$$

At the surface of the non-perfused at (i = 1)

$$\left(2\alpha_p\Delta t - \vartheta_p\right)\theta^n_{p,1} - \alpha_p\Delta t\theta^n_{p,2} - \alpha_p\Delta t\theta^n_{p,0} \qquad \textbf{(28)}$$
$$= \alpha_p\Delta t\theta^{n+1}_{p,2} - \left(2\alpha_p\Delta t + \vartheta_p\right)\theta^{n+1}_{p,1} + \alpha_p\Delta t\, \theta^{n+1}_{p,0}$$

Discretizing equations for the boundary and between the two layers: (tmax & pmax are maximum nodes of perfused and non-perfused layers respectively.

$$\frac{k}{\Delta x}\left[\theta^n_{p,1} - \theta^n_{p,2}\right] = \frac{(\theta^n_m - \theta^n_0)}{R''} \qquad \textbf{(29)}$$

$$\frac{k_p}{\Delta x}\left[\theta^n_{p,p} \quad - \theta^n_{p,p} \quad {}_{-1}\right] = \frac{k_t}{\Delta x}\left[\theta^n_{t,1} - \theta^n_{t,2}\right]$$
$$\theta^n_{p,p} \quad = \theta^n_{t,1} \qquad \textbf{(30)}$$
$$\theta^n_{t,t} \quad = \theta^n_{t,t} \quad {}_{-1}$$

For perfused layer region from (tmax-2 ≥ i ≥ 2)

$$\alpha_t\frac{\theta^{n+1}_{t,i} - \theta^n_{t,i}}{\Delta t} = \frac{\theta^{n+1}_{t,i+1} - 2\theta^{n+1}_{t,i} + \theta^{n+1}_{t,i-1} + \theta^n_{t,i+1} - 2\theta^n_{t,i} + \theta^n_{t,i-1}}{2\Delta x^2} \qquad \textbf{(31)}$$
$$- \beta\left(\frac{\theta^{n+1}_{t,i} + \theta^n_{t,i}}{2}\right)$$

The faraway boundary condition at $i = t \quad - 1$

$$(2\alpha_t\Delta t - \vartheta_t + \beta\Delta t\Delta x^2)\theta^n_{t} \quad {}_{-1} - \alpha_t\Delta t\theta^n_{t} \quad - \alpha_t\Delta t\theta^n_{t} \quad {}_{-2}$$
$$= \alpha_t\Delta t\theta^{n+1}_{t} \quad - (2\alpha_t\Delta t + \vartheta_t + \beta_t\Delta t\Delta x^2)\theta^{n+1}_{t} \quad {}_{-1} \qquad \textbf{(32)}$$
$$+ \alpha_t\Delta t\, \theta^{n+1}_{t} \quad {}_{-2}$$

Where: $\theta_t^n = \theta_t^{n+1} = 0$

Finite difference heat flux for the two-Layer compartment:

$$q_s^{n+1} = \frac{\left(\theta_{1,p}^{n+1} - \theta_s^{n+1}\right)}{\frac{\Delta x}{k_p} + R_0''} \tag{33}$$

3.EVALUATING THERMAL CAPACITANCE EFFECTS

The one-Layer compartment solution includes non-perfused layer as thermal resistance but thermal capacity effect is not included. To evaluate the effect of thermal capacitance on the two models, an example was solved with 0.381 mm of simulated non-perfused layer of Lexan and its three estimated parameters are used together with the temperature profile to test the calculated finite difference heat flux from each model. The plastic thermal conductivity and thermal contact resistance were obtained by averaging the estimated values from measurements. Thermal contact resistance of Lexan is approximately $R''_o = 6.3 \times 10^{-4}$ m^2-K/W and the thermal conductivity of the Lexan is k_L =0.596 W/m-K. The Lexan specific heat is estimated as 1260 J/kg-K and the density is 1200 kg/m^3 [17].

Table 1 indicates the corresponding three parameters for 0.381 mm-Lexan. These parameter values were used along with the temperature measurements in the two models finite-difference programs as input to generate a new set of heat flux values. Consequently, the important comparison is between the results from the two finite-difference models. Note that the thermal resistance used in the one-compartment model is $R_0^{"} + \frac{L}{k}$ and for the two-compartment model is $R_0^{"}$.

TABLE 1 THE CORRESPONDING PARAMETERS FOR THE 0.381-MM OF LEXAN MEASUREMENTS

Method	Tested values
model	
$R^{"}$	0.00138
w_b	0.051
T_{core}	36.61

4.RESULTS

The one-compartment (without thermal capacitance in plastic layer) appears to have higher values of perfusion and thermal resistance for thick layers of plastic. The effect is smaller for thinner layers of plastic.

The effect of the thermal capacitance on the heat flux can be seen in Figure 7. The original measured heat flux is plotted versus the heat flux values which calculated from the two finite-difference programs based on the measured sensor temperature curve and the parameter values from Table 1. The effect of the thermal capacitance in the plastic layer is to increase the heat flux during the initial transient portion of the curve. As indicated in Table 1, this makes the one-dimensional model appear to have higher thermal resistance and higher perfused flow. Consequently, lower values must be used to match the measured data. The resulting parameter estimation using the one-compartment model will consequently give slightly lower values of perfused flow and thermal contact resistance. This effect will be largest for the thickest plastic layers, decreasing to no effect for the thinnest layers. The two-Layer compartment finite-difference model is preferred over the one-Layer compartment finite-difference model. Figure 8 indicates that after initiating the convective cooling between the time 10 and 20 seconds, the thermal capacitance effect reduces heat flux of the one-Layer compartment model by ¼ of the two-Layer compartment model.

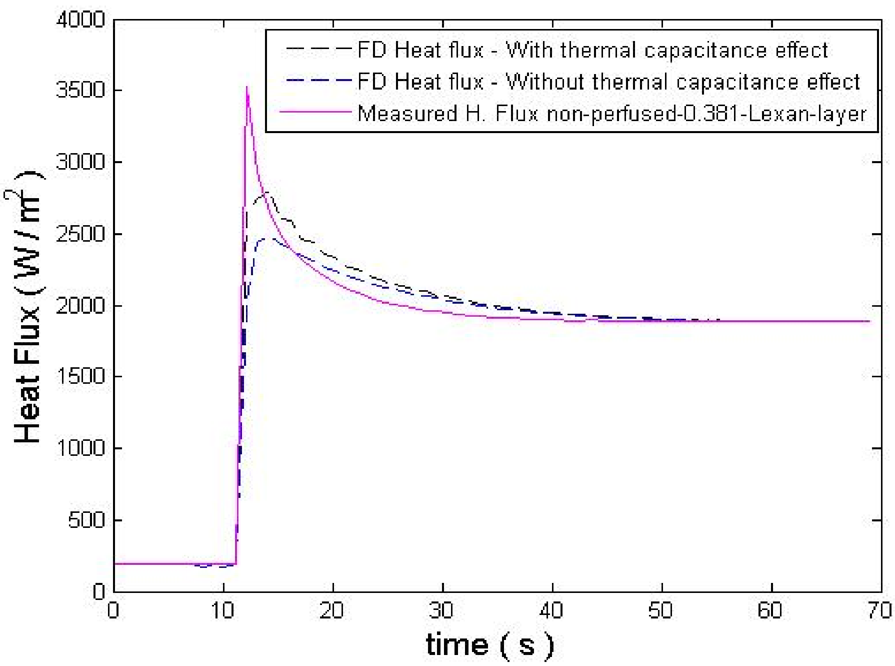

Figure 7 Heat fluxes for two models versus measured heat flux for 0.381 mm of plastic

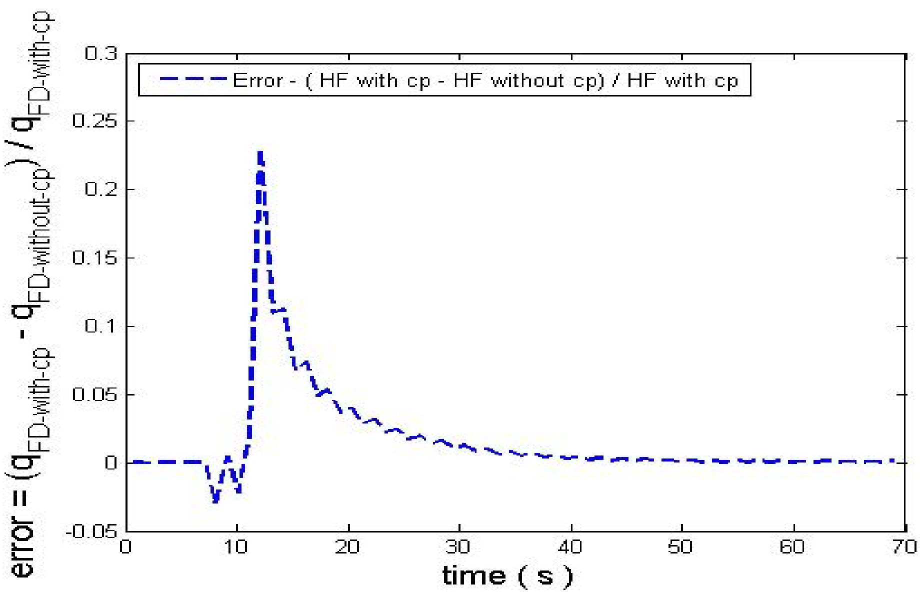

Figure 8 the error between the two finite difference models

5.CONCLUSIONS

Two mathematical models were derived to simulate heat transfer through non-perfused layer. Thermal capacitance effect was clarified to have large effect at the time of applying thermal cooling, as the studied thermal system moves away from its steady state to a transient state. Thermal capacitance represents the amount of energy which is stored during the steady state condition. The two-Layer compartment model was able to represent the energy which was stored in the non-perfused layer of plastic, while the one-Layer compartment model was not able to represent that stored energy. The one-Layer compartment model underestimates perfusion.

On the other hand, the one-Layer compartment model reduces the complexity of the system. The one-Layer compartment model does not require thickness or thermal conductivity of the non-perfused layer. An extra computational cost is associated with two-layer compartment Finite difference model, since number of meshes is greater than that require for one-Layer compartment finite difference model.

Modeling non-perfused layer with thermal resistance requires modifying estimated perfusion value to represent the right value and with that the model counts for thermal capacitance effects.

REFERENCES

[1]. Alkhwaji, Abdusalam, Vick, B., and Diller, T., “New mathematical model to estimate tissue blood perfusion, thermal contact resistance and core temperature,” Journal of Biomechanical Engineering, Vol.134, 2012, 081004, pp. 1-8.

[2]. Abdusalam Alkhwaji, Brian Vick, Tom Diller, “Modeling and Estimating Simulated Burn Depth Using the Perfusion and Thermal Resistance Probe,” Journal of Medical Device, Vol.7, September 2013, 031003, pp. 1-9.

[3]. Abdusalam Alkhwaji, Tom Diller, Brian Vick. “Detecting burn severity and the associated inflammation responses using thermal measurements in living tissue – Modeling and experimental approaches”, The 12th Annual Graduate student research symposium, May 16th, 2013

[4]. Abdusalam Alkhwaji, Tom Diller. “Monitoring and Quantifying Burn Wounds on Pig Skin using Thermal Measurements”, The International Journal of Engineering and Information Technology (IJEIT), Vol. 3, NO. 1, Dec 2016

[5]. Abdusalam Alkhwaji. “Switch Search Direction Algorithm versus GN and LM Parameter Estimation Algorithms in Modeling Inverse Heat Transfer Problem”, AL Asmarya Islamic University Journal of Theoretical and Applied Sciences, Vol. 1, NO. 1, July 2016

[6]. Boellaard, R., Knaapen, P., Rijbroek, A., Lutersema, G. J. J., and Lammertsma, A. A. 2005, “Evaluation of basis function and linear least squares methods for generating parametric blood flow images using ^{15}O-water and positron emission tomography,” *Molecular* Imaging and Biology, 7, pp. 273-285.

[7]. Petersson, J., Sanchez-Crespo, A., Rohdin, M., Montmerle, S., Nyren, S., Jacobsson, H., Larsson, S. S., Lindahl, S. G. E., Linnarsson, D., Glenny, R. W., Mure, M., 2004, “Physiological evaluation of a new quantitative SPECT method measuring regional ventilation and perfusion,” Journal of Applied Physiology, 96, pp. 1127-1136.

[8]. Montet, X. Ivancevic, M. K.., Belenger, J., Jorge-Costa, M., Pochon, S., Pechér, A., Terrier, F., and Vallé, J.-P., 2003, “Noninvasive measurement of absolute renal

perfusion by contrast medium enhanced magnetic resonance imaging," Investigative Radiology, 38, pp. 584-592.

[9]. Detre, J. A., Wang, J., Wang, Z., and Rao, H., 2009, "Arterial spin-labeled perfusion MRI in basic and clinical neuroscience," Current Opinion in Neurology, 22, pp. 348-355

[10]. Valvano, J. W., Allen, J. T., and Bowman, H. F., 1984, "The simultaneous measurement of thermal conductivity, thermal diffusivity, and perfusion in small volumes of tissue," ASME Journal of Biomechanical Engineering, 106, pp. 192-197

[11]. Khot, M. B., Maitz, P. K. M., Phillips, B. R., Bowman, H. F., Pribaz, J. J., and Orgill, D. P., 2005, "Thermal diffusion probe analysis of perfusion changes in vascular occlusions of rabbit pedicle flaps," Plastic Reconstructive Surgery, 115, pp. 1103-1109

[12]. Khan, F., and Newton, D. J., 2003, "Laser Doppler imaging in the investigation of lower limb wounds," Journal of Lower Extremity Wounds, 2, pp. 74-86

[13]. Ricketts, P. L., Mudaliar, A. V., Ellis, B. E., Pullins, C. A., Meyers, L. A., Lanz, O. I., Scott, E. P., and Diller, T. E., 2008, "Non-invasive blood perfusion measurements using a combined temperature and heat flux probe," International Journal of Heat and Mass Transfer, 51, pp. 5740-5748

[14]. Mudaliar, A. V., Ellis, B. E., Ricketts, P. L., Lanz, O. I., Scott, E. P., and Diller, T. E., 2008, "A phantom tissue system for the calibration of perfusion measurements," ASME Journal of Biomechanical Engineering, 130, 051002

[15]. Pennes, H. H., 1948, "Analysis of tissue and arterial blood temperatures in the resting human forearm," J. Appl. Physiol., 1, pp. 93-122

[16]. Butkovskiy, A. G., 1982, *Green's Functions and Transfer Functions Handbook*, Ellis Horwood Limited

[17]. von Rosenberg, D. U., 1969, *Methods for the Numerical Solution of Partial Differential Equations*, American Elsevier Publishing Company, Inc.

[18]. Mudalier, A.V., Ellis, B. E., Ricketts, P. L., Lanz, O. I., Lee, C. Y, Diller, T. E., and Scott, E. P., 2008, "Noninvasive Blood Perfusion Measurements in an Isolated Rat Liver and an Anesthetized Rat Kidney," ASME Journal of Biomechanical engineering, 130, 061013.

BIOGRAPHIES

Abdusalam Imhmed k. Al khwaji was born in Zliten /Libya, on August 23, 1972. He received B.Sc. degree in Mechanical Engineering from Omar Almukthar University, in 1996. He got M.Sc. degree in Mechanical Engineering (CSE) from Technical University of Braunschweig /Germany in 2006. Moreover, he got PhD degree in Mechanical Engineering & option in Biomedical Engineering from Virginia Tech University/USA in 2013.

After receiving his PhD, he worked as an instructor and researcher at VT, and He is currently lecturer in Department of Mechanical Engineering at AL Asmarya Islamic University/Libya. His research field is computational & experimental heat transfer and fluid dynamics, biomedical thermal instrumentation, and robot control.